\$ SUPER

Contents lists available at ScienceDirect

Dyes and Pigments

journal homepage: www.elsevier.com/locate/dyepig



Spirolactam ring locking and unlocking tuned solvent regulated unique Hg (II) sensing by a novel AIE active Rhodamine -1, 2 diamino propane-based Schiff chemosensor and its pH sensor performance

Susmita Das ^b, Manik Das ^a, Uttam Kumar Das ^b, Bidhan Chandra Samanta ^c, Arijit Bag ^d, Anutosh Patra ^e, Nandan Bhattacharya ^e, Tithi Maity ^a, *

- ^a Department of Chemistry, Prabhat Kumar College, Contai, Purba Medinipur, West Bengal, 721404, India
- ^b Department of Chemistry, School of Physical Science, Mahatma Gandhi Central University, Bihar, India
- Department of Chemistry, Mugberia Gangadhar Mahavidyalaya, Purba Medinipur, India
- d School of Natural and Applied Sciences, Maulana Abul Kalam Azad University of Technology, West Bengal, India
- ^e Department of Biotechnology, Panskura Banamali College, Panskura, West Bengal, India

ARTICLE INFO

Keywords: Rhodamine Chemosensor AIE Fluorescence study Live cell imaging

ABSTRACT

The present study highlights the development, identification, and solvent-regulated chemosensing property of a Schiff base chemosensor (E)-2-(2-((5-chloro-2-hydroxybenzylidene)amino)propyl)-3',6'-bis(diethylamino)spiro [isoindoline-1,9'-xanthen]-3-one (RBAS). The Schiff base RBAS is developed by the simple condensation of 5chloro salicylaldehyde and rhodamine-1,2 diamino propane derivative (RBAP). Interestingly this probe can optically as well as fluorometrically exhibit pH sensor activity and the spirolactam ring opening and the conversion from enol to keto form in lower and higher pH regions respectively are the main key factors to show pH sensor activity. Several spectroscopic, Dynamic Light Scattering (DLS), and scanning electron microscopy (SEM) studies confirm the AIE active property of the probe in 2:8 DMSO-water and ethanol-water mediums where the probe exhibits strong luminescence properties. Interestingly in ethanol-water and DMSO-water medium, it can detect Hg(II) via turn-on and off fluorescence respectively. Actually, in different solvent mediums, the presence of Hg(II) plays a crucial role in the spirolactam ring opening and closing of the developed probe. Simultaneously in an ethanol-water medium, it can detect picric acid by turning off fluorescence. By using mass and NMR spectrum analysis, the 1:1 stoichiometric addition of the probe and target analytes has been verified and the density functional theory (DFT) study is implemented in optimizing the probe-analyte structure. The live cell imaging study gives the approval of the biosensing ability of the probe. Impressively the probe can be successfully used to detect Hg(II) in real soil samples.

1. Introduction

Mercury has been identified as the most hazardous heavy transition metal ion to humans because its excess presence has been linked to neurotoxic, immunotoxic, and genotoxic effects [1–3]. The burning of fossil fuels, solid waste incineration, and volcanic and oceanic eruptions are the main sources of this metal ion in ecosystems [4]. Through the food chain, Hg(II) is introduced to the body, where it can build up in excess and be stored. Its very low concentration can accumulate in the human body and seriously harm the kidneys, endocrine system, brain, neurological system, and immune system [5].

Picric acid (PA), the toxic derivative of phenol, is a very powerful

explosive, which is even stronger than trinitrotoluene (TNT). It can seriously harm the human liver, eyes, skin, and respiratory systems, as well as bring chronic disorders in terms of anemia, cancer, and cyanosis [6,7]. Despite having a poisonous effect, its widespread use in industry and its high solubility in water make it easier to contaminate soil and water, creating environmental pollution. So, there is a pressing demand for simple and easy detection of these aforementioned materials.

Reliable results are obtained using contemporary analytical methods such as atomic absorption spectroscopy, chemiluminescence, and voltammetry. However, the need for complicated instruments and sample pretreatments limits their usage for online or in-field monitoring are found to be restricted [8,9]. Because of low equipment needs, ease of

E-mail address: titlipkc2008@gmail.com (T. Maity).

^{*} Corresponding author.

use, quick sensitivity, and lack of harmful potential, optical chemosensors are recommended as the right solution to this problem [10–17].

The majority of the chemosensors are not performing at their best performance as luminescent probes because of the thorny aggregation-caused quenching (ACQ) effect in molecular aggregates. Opposite to ACQ, aggregation-induced emission (AIE) showcases the photophysical phenomenon in which non-luminescent molecules in solutions with high water percentage are induced to show bright emission upon aggregate formation, as a result of restriction of intramolecular motions (RIM) caused by intermolecular steric interaction. In comparison to traditional ACQ fluorophores, the greatest advantage of the AIE active luminescence probe (AIEgens) is the highly efficient radiative transition in aggregate state for practical applications.

The AIE active luminescence probe's biggest advantage over conventional ACO fluorophores is its extremely effective radiative transition in aggregate state for useful applications and in recent years, fluorescent probes that exhibit aggregation-induced emission (AIE) have attracted a lot of attention [18-22]. Aggregation-induced emission of Schiff base molecules is pioneered by Tang et al. and this effect completely eliminated the ACQ (Aggregation-caused quenching) issue of conventional fluorescent materials [23]. In spite of the low luminescence property in the solutions with low aqueous percentages, a majestic enhancement of the fluorescence intensity is displayed by the probe as a result of aggregation in a high aqueous solution. As a result, AIE active probes that might provide fluorescence amplification rather than quenching on aggregation have emerged as a highly desirable material for reliable and quantitative sensing of several physiologically and environmentally significant target analytes. Several research groups report three types of strategies by which an AIE active probe can act to detect analysts. (1) In an optimal solvent system, in which the chemosensor exhibits the strongest emission, metal ions could be detected using the "on-off" mode [24,25]. (2) On the other hand, by inducing the AIE activity of the chemosensor in a particular solvent solution, the metal ions could be detected via fluorescence "turn-on" mode [26,27]. (3) The response of the chemosensor for the target cation with the development of metal complex with AIE activity [28]. However, one of the most important applications of this type of fluorescence enhancement probe is that in near aqueous solution, it has the capacity to detect biologically and environmentally sensitive cation and water-soluble explosives.

Due to their remarkable spectroscopic qualities of long-wavelength excitation and emission profiles and high fluorescence quantum yields, rhodamine dves have recently gained a great deal of attention in fluorescent chemosensors [29-31]. Rhodamine-based chemosensors exhibit a change in fluorescence upon binding to metal ions due to the opening/closing phenomena in the presence of metal ions. As a result, among several organic chemosensors, scientists have made larger attempts to manufacture a series of rhodamine derivatives that can be employed for quick detection and naked-eye recognition of metal ions [32,33]. The literature review reveals that hydrazine and ethylene diamine-based Schiff base chemosensors have been widely used for cation sensing [34–36]. A theoretical study unveils that the absorption spectra of 1,2 di amino propene is more or less the same with ethylene diamine. But very few reports have been found where tri carbon compound propene 1,2 di amine - Rhodamine B based chemosensor is developed for the selective detection of cations. Generally, bromo-substituted or chloro-substituted salicylaldehyde-based Schiff bases are found to be fluorescence-sensitive effective chemosensors for selective cation sensing [37,38]. Roy et al. have used 5-bromo salicylaldehyde-ethylene diamine based rhodamine derivative [39] as effective chemosensor towards target cations. But that chemosensor has no AIE active property and the chemosensor did not exhibit any pH sensor activity.

Additionally, the measurement of pH values has evolved into one of the most essential necessities with the recent advancements in biological and environmental research and Organic Schiff base compounds and their derivatives have been shown to play crucial roles in determining the pH values of a particular medium. Interestingly many rhodamine-based Schiff based have been well studied as either acid pH sensors or basic pH sensors. But no rhodamine-based Schiff base probe has been developed which can effectively act as both acid and basic sensor up to the completion of many cycles.

In the current work, one rhodamine B - propene 1, 2 di amine based chemosensor (RBAS) has been developed (see Scheme 1) which has effective Hg(II) identification ability in two AIE active ethanol-water and DMSO-water mediums via turn-on and off fluorescence response respectively. Not only that the probe can identify picric acid via turn-off fluorescence in ethanol water medium. The AIE-induced fluorescence in both mediums has been verified by DLS, SEM, UV, and fluorescence spectral studies. The total sensing phenomena have been spectroscopically monitored along with the unveiling of sensing mechanisms. HRMS analysis, ¹H NMR spectra, Job's plot, and density functional theory (DFT) calculation approve the 1:1 complexation mechanism among every probe and analyte. Interestingly the probe can act as an active pH sensor either optically or fluorometrically in both acidic and basic medium. Furthermore, the probe RBAS has been successfully used as a biosensor and in the detection of the Hg(II) in real soil samples.

2. Results and discussions

2.1. Synthesis, IR, UV and ESI-MS analyses of the rhodamine-1,2-diamino propane derivative (RBAP) and RBAS

The probe RBAS, (E)-2-(2-((5-chloro-2-hydroxybenzylidene)amino) propyl)-3',6'-bis(diethylamino)spiro[isoindoline-1,9'-xanthen]-3-one has been developed through the condensation reaction of rhodamine-1,2-diamino propane derivative (RBAP) with 5-chlorosalicylaldehyde and the subsequent spectral studies have been implemented for proper identification of the probe. The FTIR spectrum data are used primarily to gain a preliminary understanding of the structural skeleton. In the spectrum of RBAP (Fig. S1 in supporting information file) the peaks at 2969 cm-1, 1686 cm⁻¹ and 1614 cm⁻¹ appear as a result of C-H stretching, C=N stretching, C=O stretching. In probe, RBAS all three aforementioned stretchings appear in 2969 cm⁻¹, 1682 cm⁻¹ and 1617 cm⁻¹ respectively (Fig. S2 in supporting information file). The sharp band in 1512 cm⁻¹ and 1510 cm⁻¹ for **RBAP** and **RBAS** respectively can be attributed to the vibration of skeletal benzene in the probe. The electronic spectra of RBAP show two absorption bands at around 275 nm, 320 nm which is attributed to the n- π^* and π - π^* transition whereas these two transitions appear at 272 nm, 318 nm for RBAS (Fig. S3).

The Electrospray Ionization Mass Spectra (ESI-MS) (positive mode, m/z up to 1200 amu) of **RBAP** and **RBAS** are recorded in methanolic solutions (Figs. S4 and S5 in supporting information file). **RBAP** and **RBAS** show one peak at m/z = 499.3065 and m/z = 638.2958 which is assigned for the species [**RBAP** + **H**]⁺ (calculated m/z = 499.6590) and [**RBAS** + **H**]⁺ (calculated m/z = 638.2201) respectively. Figs. S6 and S7 represent the ¹H NMR of **RBAP** and **RBAS** whereas Figs. S8 and S9 represent the ¹³C NMR of both compounds. The details of NMR characteristic signals are given in the experimental section of the manuscript.

2.2. Crystal structure of RBAP

The colorless block-shaped X-ray quality single crystals of the compound is crystallized in a centrosymmetric 'triclinic' space group 'P-1' from DMSO solvent system by slow evaporation at room temperature. The asymmetric unit of the crystal contains one molecule. strong aromatic CH ... Π interaction (3.331 Å, calculated using mercury 3.3 software) and CH···O interactions (C···O distance 3.544 Å, \angle C-H-O = 161.97°, calculated using mercury 3.3 software) present in the crystal (Fig. 1A) that resulted in the overall crystal packing (Fig. 1B). The molecular plot of the crystal is given in Fig. 1C.

Scheme 1. Synthesis of RBAP and RBAS.

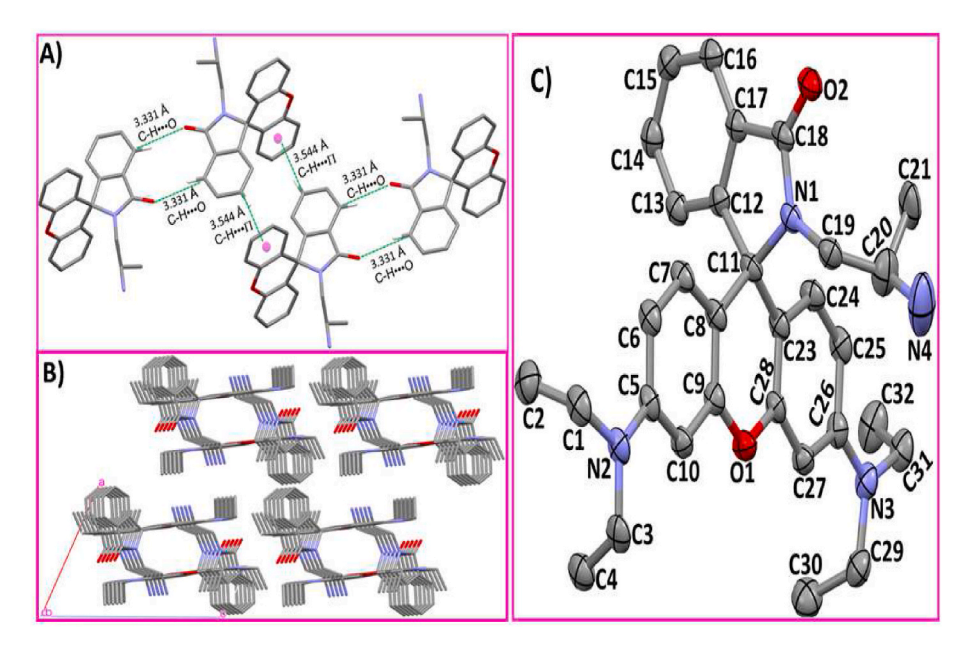


Fig. 1. A) Aromatic CH ... Π interaction and CH···O interactions have been shown. For better clarity diethyl amine moieties (side chain) have been attached to the aromatic ring and all the hydrogen atoms were hidden. B) The overall parallel packing is shown along axis-b (for better clarity, all the hydrogen atoms were hidden).

C) The molecular plot of the crystal (for better clarity, all the hydrogen atoms were hidden).

2.3. Crystal structure of RBAS

The X-ray quality crystal of the **RBAS** was crystallized in the centrosymmetric triclinic space group '*P-1*' from methanolic solution of that compound. The asymmetric unit contains single molecule of the compound. The imine group of the ligand is involved in intramolecular hydrogen bonding [N(9) ... H–O(1) = 1.88 Å, \angle NHO = 147.1°] with the phenolic –OH group (Fig. 2A & Table S1). There are also various intermolecular C–H···O interactions (O···H–C = 3.591–3.284 Å, \angle CHO = 166.9°–129.9°, Fig. 2B & Table S1) present. These intramolecular hydrogen bonding and intermolecular C–H···O interactions produces overall packing (Fig. 2C) of the stable crystal structure. The molecular plot of the crystal is given in Fig. 2D.

2.4. Photophysical property

The developed **RBAS** contains a proton transfer moiety, so it is expected that the molecule is dominated by a combination of locally excited state (LE), and excited-state intramolecular proton transfer (ESIPT). To scrutinize the emission mechanism, the photophysical behavior of **RBAS** has been checked in different solvents with polarity differences and Fig. S10 displays the total results. The molecule [2 μ M] exhibits dual fluorescence emission in different solvents. The shorter wavelength peaks have been assigned to the locally excited state (LE), which is due to the vibrational signatures of the molecule whereas the broad peak in longer wavelength may be due to the ESIPT process since this molecule contains an –OH group (can contribute ESIPT). From the crystal structure, it is seen that the H atom of -OH can participate in

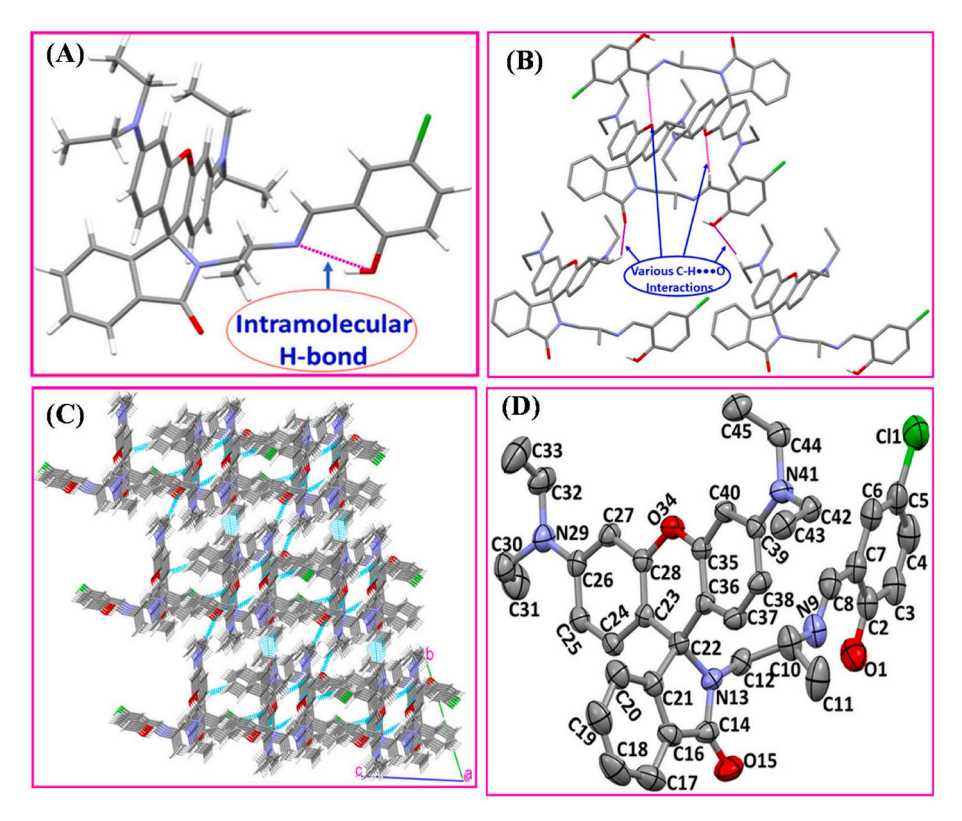


Fig. 2. A) The intramolecular hydrogen bonding; B) All the possible CH···O interactions present in the crystal packing and (for better clarity, all the hydrogen atoms were hidden, except H-atom participated in the interactions. C) The overall parallel packing has shown along axis-a D) The molecular plot of the crystal (for better clarity, all the hydrogen atoms were hidden).

intra-molecular H-bonding with the N atom forming one six-member ring and the donor accepter bond length and angle $[O(1)-H(1) \dots N(9)]$ (Table S1 in the supporting information file) confirms the moderate H-bonding. So, there is a possibility of the ESIPT process. With the

change of solvent polarity, the red shift of the spectral position and the intensity change (high to low) of the tautomer band in nonpolar to protic solvents approve the presence of ESIPT behavior (Fig. S10), and this behavior is correlated to the disruption of intramolecular hydrogen

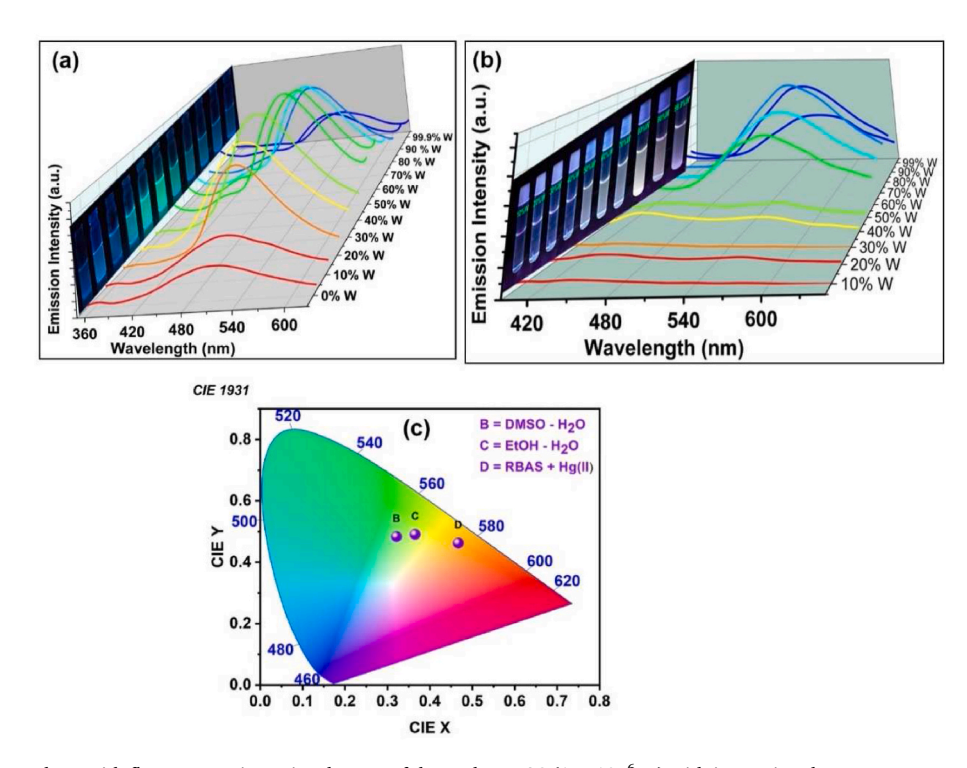


Fig. 3. The optical changes along with fluorescence intensity changes of the probe RBAS (1×10^{-6} M) with increasing the water percentage from 0 % to 99.99 % in (a) DMSO-water (b) EtOH-water AIE active medium (c) Chromaticity diagram from Fluorescence spectra.

bonding through intermolecular hydrogen bonding using protic solvents. In the presence of a high concentration of water intermolecular H-bonding occurs leading to a rigid aggregate formation.

2.5. AIE performance of RBAS

The photophysical feature of RBAS is scrutinized by checking its fluorescence response in the ethanol-water and DMSO-water mixture by varying the water content from 0 % to 99 % and the recorded data has been condensed in Fig. 3. The probe is fully soluble in both Ethanol and DMSO and its solubility in water is not at the expected level. So, anybody can say ethanol/DMSO is a good solvent for RBAS whereas water is a bad solvent. The probe remaining in the ($f_w \le 10$ vol%) good solvents show a weak fluorescence emission at 563 ($\Phi = 0.002$) nm 506 nm ($\Phi =$ 0.003) in ethanol-water and DMSO-water medium respectively. But with incremental addition of water volume from 50 % to 80 % the remarkable synchronous enhancement of emission intensity at 540 nm $(\Phi = 0.172)$ is visualized along with a distinct color change in ethanolwater medium but in DMSO water medium the enhancement of fluorescence intensity at 526 nm ($\Phi = 0.183$) with optical color changes is visualized with increasing the water percentage up to 80 % (Fig. 3). The fluorescence lifetime of the probe has been measured for aggregate in ethanol/water and DMSO-water medium [30 $\mu M]$ (fw = 30 % and 80 %), (Fig. S11 in the supporting information file), and Table S2 in the supporting information file summarizes the lifetime changes. The fluorescence lifetime in the presence of 80 % water is higher than in the presence of 30 % water suggesting the AIE behavior of the probe.

Such kinds of fluorescent behavior of **RBAS** can be attributed to the change of molecular packing modes and conformations in the aggregated states [40,41]. At the same time **RBAS** is largely isolated with little interaction with other neighboring **RBAS** in both ethanol and DMSO medium. As a result, the single bond rotation and high amplitude vibrational modes are the key factors for the dominant nonradiative decay channel which leads to the lower fluorescence intensity. In the presence of high-water content, the single bond rotations are completely locked in the aggregated state, arising as a result of intermolecular interactions and this phenomenon promotes molecular planarity and strengthens the π -conjugation of **RBAS**, leading to a red shift in the emission maxima. we can speculate that such kinds of emission spectral change are accredited to the emission from J-aggregates [42].

The emission intensity of **RBAS** in different AIE states can be visualized in CIE 1931 diagram (Commission International de L'Eclairage) (Fig. 3c). From fluorescence spectral data the CIE coordinates are found to be at (0.32, 0.48) and (0.36, 0.49) in EtOH – H_2O and DMSO – H_2O systems respectively.

Fig. S12 displays the UV–vis absorption spectrum changes of **RBAS** in the presence of different percentages of water. The pictograph exposed that the probe shows two absorption maxima at 277 nm and 315 nm when 10% of water is present in ethanol solution whereas in DMSO-water medium (10 % water) the probe also displays two absorption maxima at 273 nm and 318 nm. But after increasing the water percentage (up to 80 % in both DMSO and ethanol) in both cases this maximum gradually decreases with a redshift of the spectral position along with the development of a new band at 408 nm in DMSO water medium (indication of J-aggregates in both the medium). This observation gives strong support behind the development of the new materials as a result of the perfect aggregation effect of the probe when the water percentage is high.

The DLS (Fig. S13 in the supporting information file) results show that the size of the particle increases with increasing water percentage in ethanol-water and DMSO-water respectively.

SEM study also reveals that **RBAS** molecules aggregate to form a basket-like structure at room temperature (Fig. S14 in supporting information file).

2.6. pH effect of RBAS

For checking the pH sensor activity of the target probe, the fluorescence response of **RBAS** solution has been thoroughly investigated at different pH values. The pH of the solutions is adjusted by using HCl and NaOH solutions.

The experimental results which are summarized in Fig. 4 and Fig. S15 elucidate that the compound **RBAS** shows a strong orange fluorescence color near 589 nm in an acidic solution (pH \leq 4). Actually, in the lower pH, the spirolactam ring opening of the mother molecule occurs [40] whereas at the higher pH of the solution, the spirolactam ring again closed. With decreasing the pH value of the solution, a continuous enhancement of the color intensity and fluorescence intensity is visualized.

The pH sensitivity of the target chemosensor in an acidic region is similar to the previously reported other rhodamine-based pH sensors [43-46]. But in the present scenario, our developed material comes to the leaderboard with a marvelous advancement. Here with increasing the pH value of the RBAS solution (pH > 8) (Basic solution) a new emission band near 465 nm is visualized along with the distinct color change from colorless to bright cyan color (see above) and the enhancement of emission intensity as well as the intensity of the color is gradually increases up to pH = 13. In higher pH, the "ESIPT" character (discussed above) will be dominative, which boosts the enol - emine to keto - amine conversion, leading to the introduction of emission intensity to the material. At the same time, the ICT proceeds with the ionization of the hydroxyl group, leading to the development of an intense green color. This color-changing behavior of the RBAS with the change of pH can be repeated in several cycles simply by altering the pH of the practical solution (Fig. S16). The emission intensity, quantum yield, and wavelength variation of the probe with the change of pH are condensed in Table S3. So the spirolactam N and hydroxyl group are the two parts for exhibiting pH sensor activity. The pH response of the probe in terms of color, emission intensity, and wavelength variation and quantum yield is schematically represented in Scheme 2. All the above discussions approve one fact that in the future the probe may be a strong competitor among the fluorescence pH marker community.

2.7. Analytical performance of the probe RBAS towards competitive cations

2.7.1. Optical signature

As the probe, **RBAS** is an AIE active material in DMSO-water and ethanol-water mediums so its performance as a chemosensor has been inspected in the detection of several cations in both the AIE active

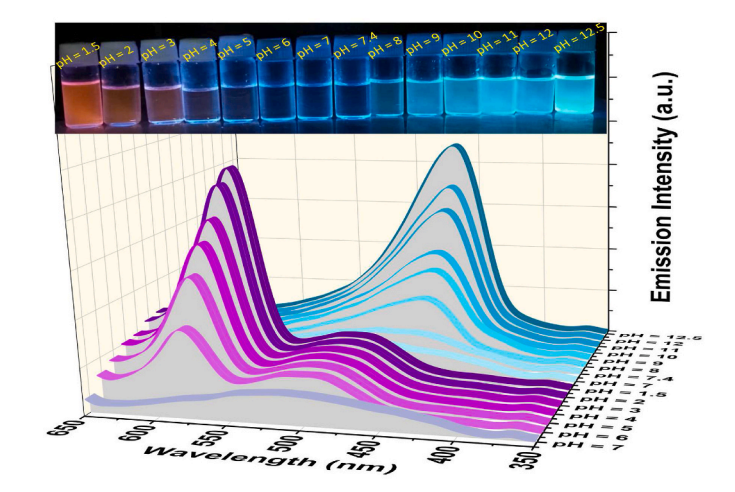
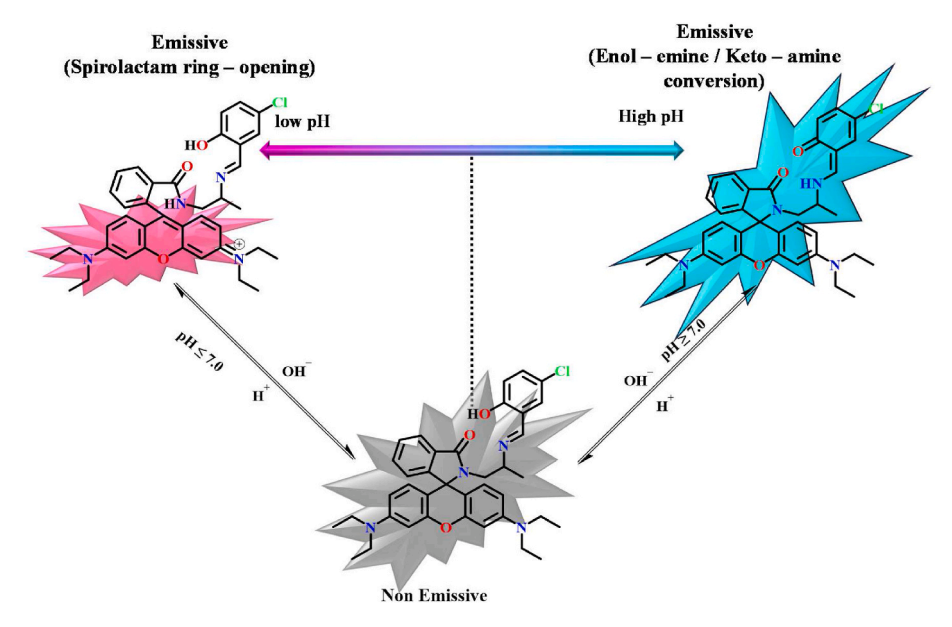


Fig. 4. Optical and the emission intensity change of RBAS (1 \times 10^{-6} M) by altering the pH of its solution.



Scheme. 2. Proposed mechanism for the conformational changes od RBAS under the influence of different pH (acidic and basic).

mediums. Initially, the investigation starts with the optical color change of **RBAS** in the presence of different cations, like Al(III), Fe(III), Cr(III), Mn(II), Co(II), Zn(II), Ni(II), Cd(II), Hg(II), Na(I), K(I), Co(II), Mg(II), and Ca(II) in both the medium.

In this study, the optical color changes of **RBAS** (3×10^{-6} M) solution are visualized in the presence of different competitive cations. Under the UV light in 2:8 DMSO-water medium, the intense green color solution of the probe shifts vividly to colorless in the presence of only Hg (II) ion (1.5×10^{-5} M). Here one special fact is noticeable that after a long time, a light pink color solution is developed (see Fig. 7b). On the other hand in an ethanol-water AIE active medium, a deep pink color solution is observed instantly only in the presence of Hg(II) (Fig. 5). Impressively no distinct color change is observed for other competitive cations in both the medium.

2.7.2. Fluorescence spectroscopic response

After optical signature checking, the fluorescence response of the studied probe is scrutinized with the separate presence of the competitive cations. Fig. S17 displays the fluorescence response of RBAS (3 \times 10^{-6} M) towards several cations in different AIE active mediums. The

pictograph shows that in ethanol-water and DMSO-water AIE active mediums, the probe RBAS (3 \times 10 $^{-6}$ M) exhibits strong emission at 540 nm ($\phi=0.183$) over excitation at 326 nm and at 526 nm ($\phi=0.172$) over excitation at 320 nm respectively. Interestingly, in the ethanol-water medium after the separate addition of various cations to the probe, the enhancement of the fluorescence intensity is observed in the presence of only Hg(II) (1.5 \times 10 $^{-5}$ M) whereas, in DMSO water AIE active medium, the probe shows the reduction of emission intensity in presence of Hg(II) only. Additionally, the turn-on Fluorescence of Hg(II) in the EtOH - H₂O system can be visualized in CIE 1931 diagram (Commission International de L'Eclairage) (see above in Fig. 3c) where CIE coordinates are found at (0.46, 0.463), indicating the appearance of emission of RBAS - Hg(II) towards the orange-red region.

After the optical and fluorometric response, the absorbance variance of the **RBAS** has been recorded after gradual additions of Hg(II) to ethanol-water and DMSO-water AIE active mediums (Fig. 6).

Both the titration pictographs exhibit that in 2:8 ethanol-water medium, the probe **RBAS** displays two absorption bands centered at 278 nm, and 326 nm whereas in 2:8 DMSO-water medium, it also shows the two absorbances at 275 nm and 320 nm. The separate incremental

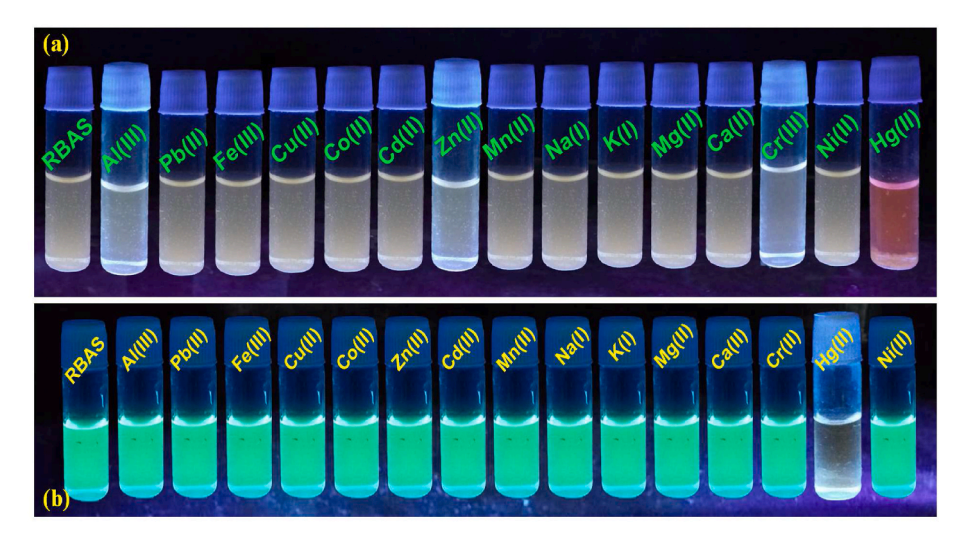


Fig. 5. Optical change of color of **RBAS** after the addition of several cations (1:5) in a 2:8 a) ethanol/water b) DMSO-water medium showing the distinct color change only in the presence of Hg(II).

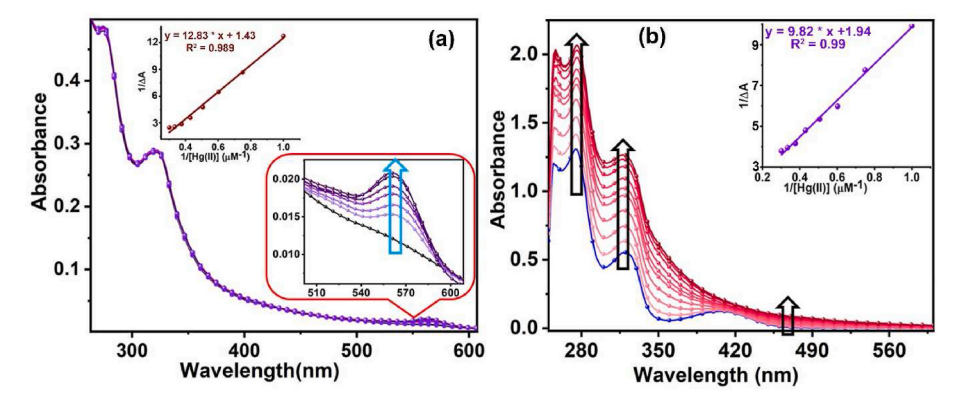


Fig. 6. The absorbance change of RBAS (2×10^{-6} M) after gradual addition of Hg(II) in a) 2:8 ethanol-water medium b) 2:8 DMSO-water medium [Inset: the binding constant measurement graph.

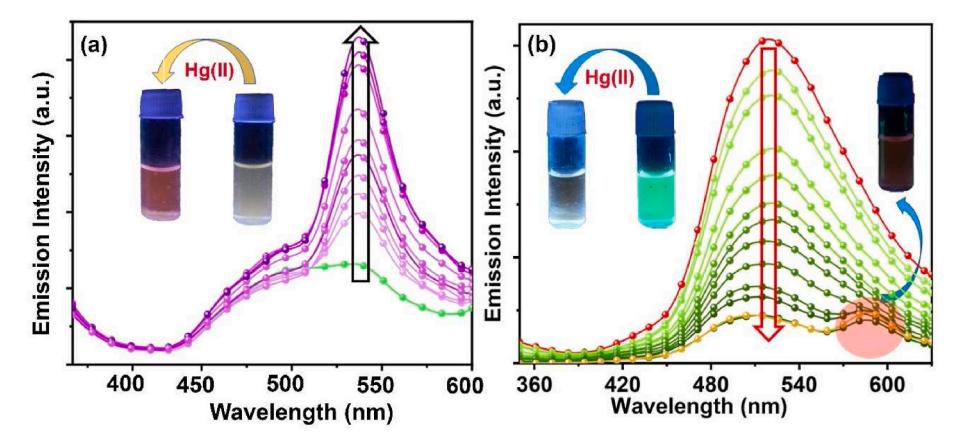


Fig. 7. Fluorescence intensity changes of RBAS (3×10^{-6} M) upon incremental addition of Hg(II) (1.0– 25.0×10^{-5} M) in a) ethanol-water b) DMSO-water medium. Inset: optical colour change upon addition of Hg(II) to RBAS solution.

addition of Hg(II) to the probe a steady enhancement in all the absorbances is visualized in ethanol-water and DMSO-water medium along with the development of a new peak at 560 nm and 480 nm respectively.

By using B–H equation, (equ. 1) the calculated binding constants for RBAS – Hg(II) adducts are 1.11 \times 10^5 M^{-1} , 1.97 \times 10^5 M^{-1} in ethanolwater and DMSO – water respectively.

$$\frac{1}{A - A_0} = \frac{1}{(A_{max} - A_o)K_b \times C} + \frac{1}{(A_{max} - A_0)}$$
 (1)

The stability of the probe in ethanol-water AIE active medium has been authenticated by recording the absorbance changes of the probe as a function of time (Fig. S18) and the results show that the probe is fully stable in AIE active medium as very little absorbance change is visualized with the change of time.

Followed by the optical, UV metric, and fluorometric confirmation of the selective detection of Hg(II) by RBAS, a quantitative evaluation comparing the fluorescence intensity change of the probe as a function of the concentration of analyte in both working mediums has been conducted. It is quite clear from the titration data summary (Fig. 7) that the RBAS exhibits a very strong emission at 540 nm ($\Phi=0.172$) and 526 nm ($\Phi=0.183$) in ethanol-water and DMDO-water medium respectively.

After consecutive incremental addition of Hg(II) to **RBAS**, the fluorescence intensities of **RBAS** steadily increase ($\Phi=0.269$) in ethanolwater medium (Fig. S11) whereas a gradual reduction of the emission intensity is observed in DMSO-water medium ($\Phi=0.089$) along with the development of a new peak during the ending part of titration. This observation indicates that after a certain period of time, an enhancement of fluorescence intensity is observed in a higher wavelength. This

observation is explained in the mechanism unveiling section.

In the presence of Hg(II) in RBAS in DMSO-water AIE medium no remarkable change in lifetime is observed (Fig. S11 in the supporting information file). The fluorescence quenching in the presence of Hg is static as in the presence of S $^-$ the quenching can be recovered and this type of quenching leads to the negligible change in fluorescence lifetime. But in the presence of Hg in ethanol-water AIE active medium the lifetime increases and the development of new fluorescence active Hg(II) complex with RBAS probe having spirolactam ring opening structure, leads the enhancement of lifetime (Fig. S11 in the supporting information file)

The limit of detection (LOD) is measured by utilizing the equation (equ. 2)

$$LOD = 3 \sigma/K$$

Where σ is the standard deviation of the blank solution and K is the slope between the fluorescence versus each analyst's concentration. LOD is measured to be 2.43×10^{-8} M and 4.54×10^{-8} M in DMSO-water and ethanol-water respectively (Fig. S19 in supporting information file). By utilizing the fluorescence titration pictograph, the binding constant K has been measured from a linear fitting plot by utilizing the following equation (equ. 3) where the binding constant K has been measured from the intercept.

$$\log \frac{F - F_{min}}{F_{min} - F} = \log K + n \log[M] \tag{3}$$

The binding constant values for RBAS-Hg(II) are measured to be $1.318\times10^5\,M^{-1}, 2.13\times10^5\,M^{-1}$ (Fig. S20) in EtOH – water and DMSO-water respectively.

In the effective chemosensor development research field, reproducibility is a crucial factor for the actual implementation of a chemosensor. Here, the presence of the reversibility has been accomplished by the alternative addition of sodium sulfide (Na₂S) and Hg(II) to **RBAS**-Hg(II) adduct (Fig. S21). Finally, the results of the competitive assay study prove that among several competitive cations only Fe(III) and can slightly interfere with the turn-on and off fluorescence response of **RBAS** in the presence of Hg(II) (Fig. S22).

2.8. Picric acid (PA) sensing efficacy of RBAS

In an ethanol-water AIE active medium, the probe is exposed to check its picric acid sensing ability. Initially, in 2:8 ethanol-water medium, the cream color of the probe **RBAS** (3×10^{-5} M) turns colorless when exposed to UV light after the addition of four equivalents of picric acid (Fig. 8 and Fig. S23) and for other nitroaromatic compounds (NACs), no distinct color change of the probe is observed.

Following that, electronic titration and fluorescence titration in the same working medium are implemented to further monitor the picric acid detection phenomena. Fig. 8 displays the summary of the titration results.

The pictograph discloses that the bare **RBAS** (2×10^{-6} M) shows two absorption maxima at 278 nm and 326 nm, which steadily increase upon the addition of picric acid (1– 20×10^{-6} M) solution. but the incremental order is higher at 328 nm compared to 277 nm. The measured probeanalyte binding constant is 5.49×10^4 M $^{-1}$ (inset of Fig. 8a). Simultaneously, in the same medium after the gradual addition of picric acid (2– 30×10^{-6} M) to **RBAS** (2×10^{-6} M), an impressive decrease in emission intensity is seen. The LOD value has been determined as 8.37×10^{-8} M (Fig. S24). The spectroscopic results approve the sensing ability of **RBAS** to picric acid.

After the photophysical property study as well as chemosensor activity study of **RBAS** one can easily say that **RBAS** is not a simple added molecule in the rhodamine-based chemosensor library. To support this statement we can say that for the first time, one rhodamine-based chemosensor can show both acid and base sensor activity, AIE activity in DMSO-water and ethanol-water medium, Hg(II) sensing in both AIE active medium via turn-on and turn off response and picric acid sensing activity in AIE active medium. To validate this point Table S4 is

incorporated in the supporting information file which discloses a comparative property of several rhodamine-based Schiff base chemosensors.

2.9. Possible probe-analyte sensing mechanism

The foregoing discussion makes evident the recognition of Hg(II) and picric acid by the newly developed probe RBAS. Now, it is time to disclose the probe-analyte binding mechanism (Scheme 3). In a 2:8 ethanol-water AIE active medium, the spirolactam ring opening occurs in the presence of Hg(II), inducing the fluorescence response with high intensity. In the presence of ethanol (protic solvent), the ring opening becomes easy.

Here the high polar ethanol medium helps to perform ring opening. But in 2:8 DMSO-water AIE active medium, upon addition of Hg(II) a fluorescence quenching (Fig. 7) is observed and this behavior is attributed to chelation-enhanced quenching (CHEQ) effects and the less polar DMSO medium initially fails to open the ring in presence of Hg(II). In the DMSO-water medium, the presence of Hg(II) can form a complex between Hg(II) and the probe, and the Hg complexation with the surface molecule of the probe induces spin-orbit coupling mechanism [due to the presence of heavy Hg(II)] to depopulate the emissive S1 state of the molecule which leads to the reduction of emission intensity of AIE active gen. Interestingly after a long time and in the presence of a high concentration of Hg(II) the ring opening occurs and this is confirmed in a quantitative fluorescence assay study where in the finishing time of titration a new emission intensity band is further developed in higher wavelength and light pink color is visualized (Fig. 7).

Implementation of the traditional Job's plot method assures the probe–analyte 1:1 stoichiometry complexation in both DMSO-water and ethanol-water mediums. (Fig. S25).

2.10. Mass spectral analysis

The mass spectral data analysis gives strong support against the 1:1 coordination of probe and analyte. After separate mixing of probe **RBAS**-Hg(II) in mass spectra, we get one major peak at m/z=873.2227 which is assigned for the species [C₃₈H₄₀HgCl₂N₄O₃](calculated 873.2250), in both system (Fig. S26).

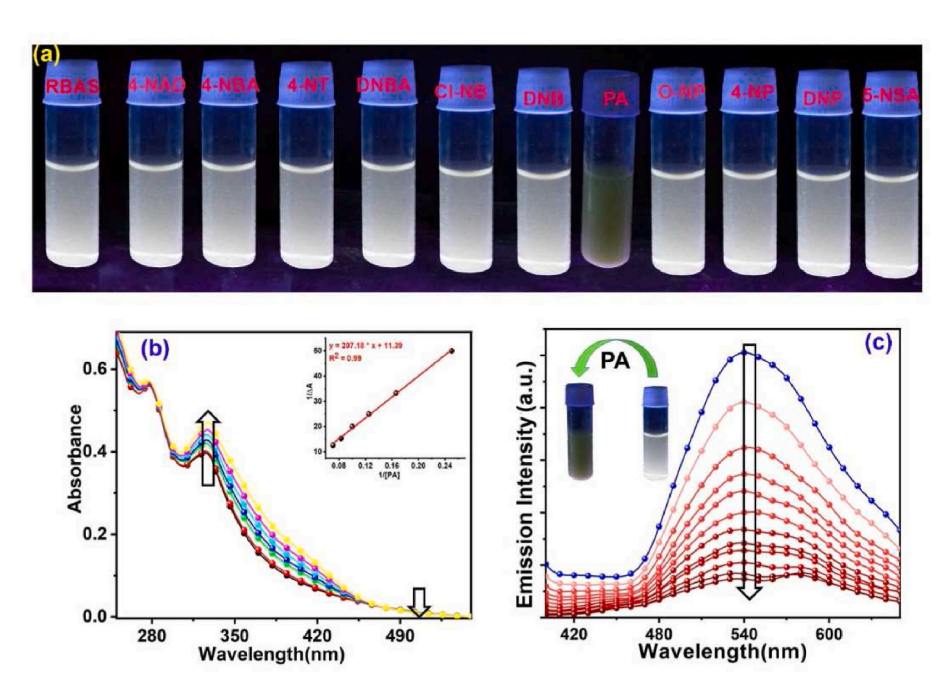
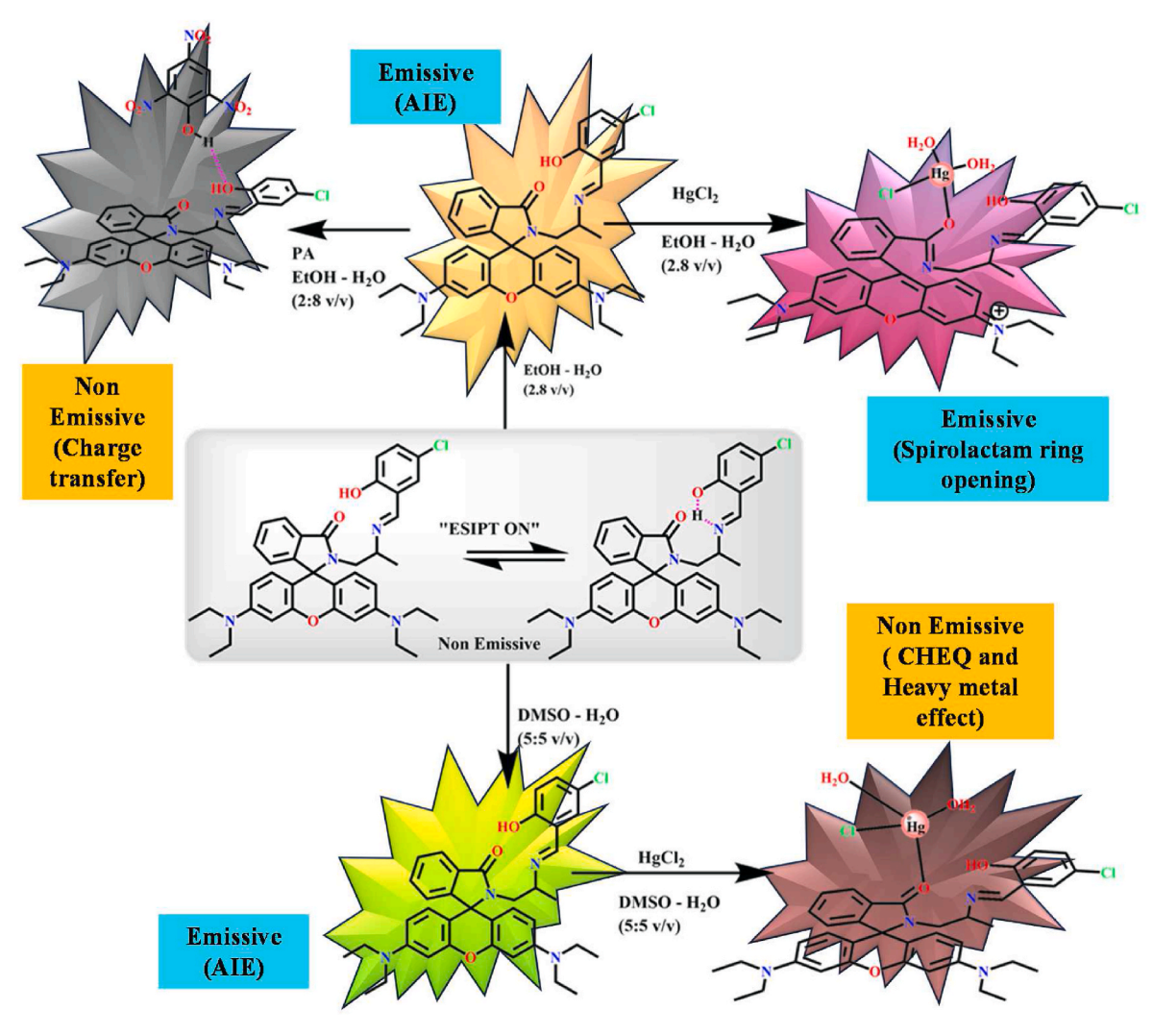


Fig. 8. (a) Optical color change of RBAS in the presence of four equivalent picric acid (b) absorbance change of RBAS in the presence of picric acid (c) fluorescence quenching of RBAS in the presence of picric acid.



Scheme 3. Possible mechanism of the sensing of Hg(II)/picric acid by RBAS in different AIE system.

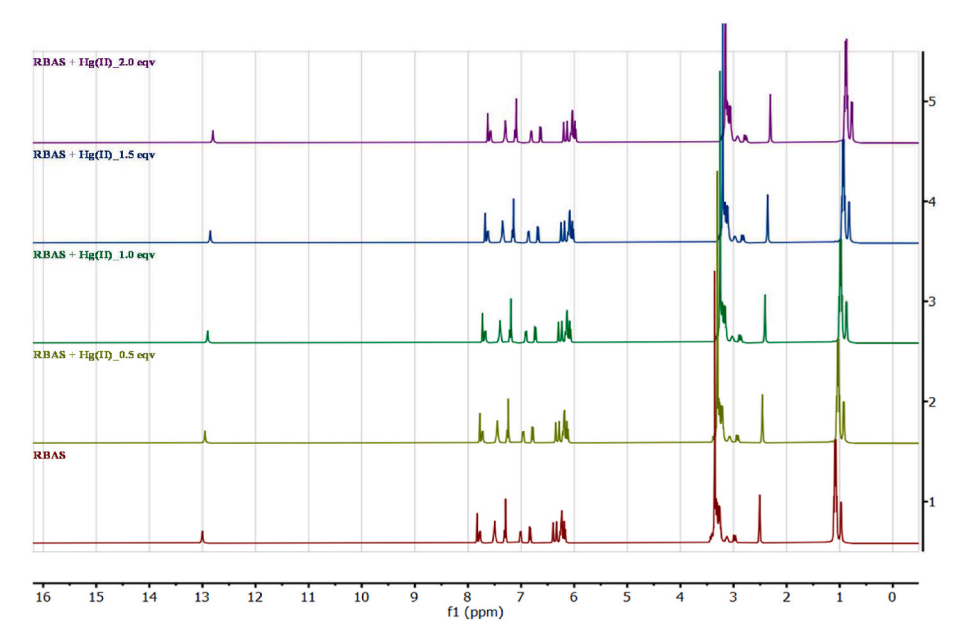


Fig. 9. NMR titration of RBAS by Hg(II).

2.11. NMR titration

Furthermore, ¹H NMR spectral titration also validates the Hg(II) coordination with **RBAS**. The ¹H NMR spectrum of the probe are recorded in the presence of different concentration of Hg(II) and the spectral titration is represented in Fig. 9.

NMR spectrum unveils that all the aromatic protons and aliphatic protons of the probe appear in the region of 6.2–7.8 ppm and 1.1–3.5 ppm and the aromatic OH group appears at 12.9 ppm.

During Hg(II) complexation, the probe **RBAS** acts as an N, N donor bi-dented ligand where the phenoxide group does not coordinate to the metal center and this can be clearly seen in the NMR spectrum where the signal of the aromatic OH proton present on all the spectrum and the shifting of aromatic and aliphatic protons confirms the formation of metal-ligand complexation.

2.12. DFT study

After getting confirmation regarding the formation of 1:1 RBAS-analyte complexation DFT study has been performed to optimize the structure of the probe as well as probe-analyte complexes in both the medium. The optimized structure of RBAS and the complexes are depicted in Fig. S27. From the optimized structure it is observed that in the Hg complex, the Hg atom is coordinated by one O atom from RBAS, two O from water, and one Cl⁻ atom to form a distorted tetrahedral geometry.

We computed the TDDFT spectra of the **RBAS** and the **RBAS** – Hg(II) complex in both EtOH and DMSO solvents separately at room temperature. The HOMO – LUMO energy gaps are summarized in Fig. 10. The results unveil that the HOMO – LUMO gap for the sensor **RBAS** is found to be 3.19 eV in the DMSO medium and 3.17 eV in the EtOH medium. For **RBAS**- Hg(II) complex the HOMO – LUMO energy gap is measured to be 1.57 eV and 1.62 eV in EtOH and DMSO system respectively. Besides **RBAS** – PA, the HOMO – LUMO energy gap is found to be 1.40 eV in

EtOH system. The theoretical absorption spectral bands with their electronic transitions and oscillation strengths are tabulated in Table S5.

In EtOH solvent, **RBAS** exhibits two absorption bands at 272.86 a.m. and 316.18 nm while in experimental spectra these peaks are found to be 272.09 nm and 318.05 nm which are well matched to the theoretical spectra. The spectrum band arises at 316.18 nm due to the electronic transition from S_0 to S_1 between the HOMO bonding molecular orbital to LUMO antibonding molecular orbital (Electron density shifts towards the C—N imine bond and the aromatic part of the aldehyde moiety.

For Hg Complex in EtOH solvent, two distinct spectral bands are found at 274.95 nm and 320.48 nm showing a good agreement with the experimental result. The band arises at 320.48 can be ascribed to the $\rm S_0$ to $\rm S_7$ electronic transition between the HOMO-3 to LUMO molecular orbital.

In the DMSO solvent, the absorption bands are found to be 272.46 nm and 325.10 nm which has well matching with the experimental findings. The Band arises at 325.10 nm and could be assigned to S_0 to S_{13} electronic transition between the HOMO-6 to LUMO molecular orbital. In Both cases the electron density shifts from the xanthene part of the Rhodamine spirolactam ring to the aromatic part of the aldehyde moiety.

For **RBAS** – PA adduct in EtOH solvent, the theoretical spectral bands are 280.13 nm and 329.71 nm whereas the experimental bands are located at 277.19 nm and 328.39. The absorption band that arises at 329.71 nm could be assigned to the electronic transition S_0 to S_6 between the HOMO-1 to LUMO+2 molecular orbital (electron density shifts from the xanthene part of the Rhodamine spirolactam ring to the PA moiety).

In this experiment, the calculated low-energy gap values after the metal complex formation from the ligand support the spectral red shift for each complex in the experimental procedures and these results display favorable agreements with the above discussions.

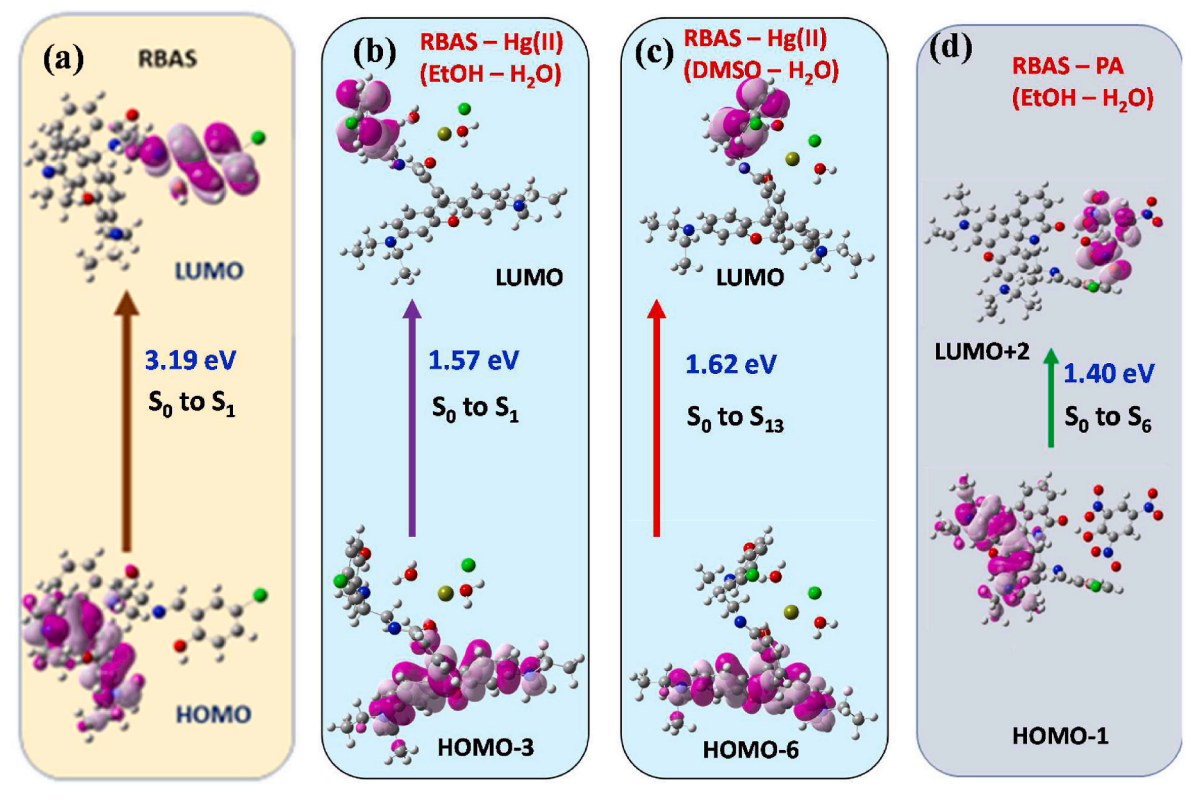


Fig. 10. HOMO-LUMO energy gap of RBAS, RBAS-Hg(II) complex, and RBAS-picric acid complex.

2.13. Live cell imaging study

After spectroscopic monitoring of Hg(II) sensing phenomenon by **RBAS**, the bio-sensing ability of the probe has been checked by performing a cell imaging study. Before the cell imaging study, there is an urgent need to check the cell viability study of the target probe.

Fig. S28 displays the cell viability study of the probe indicating the disability of cytotoxicity up to 100 μM concentration. In the cell imaging study initially, the HeLa cells are first incubated with **RBAS** for 4 h and after that, the cells are treated with Hg(II) (1: 4 ratio) ions for an additional 2 h. Interestingly the cells treated with the bare **RBAS** show intense green fluorescence but impressively the green fluorescence disappears after the addition of Hg(II) (Fig. 11). This observation clearly indicates that **RBAS** can readily cross the membrane barrier of the cells, and it can rapidly recognize Hg(II) within the cell.

2.14. Application in soil sample detection

The soil samples including sandy soil, Humas soil, and Alluvial soil are collected from different locations nearest to our institute. The fluorescence responses of Alluvial soil at different concentrations of Hg(II) are investigated under UV light ($\lambda_{\rm ex}=365$ nm) as well through fluorescence spectra. The results which is pictographically represented in Fig. 12 unveil that the concentration change of Hg(II) in soil is easily detected by the probe RBAS by changing its fluorescence color as well as spectral change. That means with increasing the concentration of Hg(II) the color of the solution becomes more intensified and the emission intensity also increases. All these results represent a strong evidence that the chemosensor RBAS may be an efficient practical chemosensor for recognition the Hg(II) in several types of real samples.

3. Conclusion

In the present study, a novel Schiff base **RBAS** has been developed by simple condensation of 5-chlorosalicylaldehyde and rhodamine b-1, 2-diamino propane derivative (**RBAP**). The spectroscopic data and single crystal data analysis of **RBAP** and **RBAS** properly identify both compounds. After the acknowledgment, the Schiff base chemosensor **RBAS** is used to check its pH sensing and chemosensing behavior. A thorough optical and fluorometric inspection proves the acid-base pH sensor activity of **RBAS** up to many cycles. The enol-keto transformation in basic medium and spirolactam ring opening in acid medium is mainly responsible for exhibiting such pH sensitivity. Further investigation shows that the probe also shows AIE-induced fluorescence response in ethanol-water and DMSO water medium. With the presence of 80 % water, the probe shows the highest emission intensity in ethanol-water

and DMSO-water medium with a distinct color which is authenticated by fluorescence spectroscopic, UV spectroscopic, DLS, and SEM studies. The AIE active behavior of the probe has been successfully utilized to detect Hg(II) via turn-on and off fluorescence response in ethanol-water and DMSO water respectively. On the other hand, in an ethanol-water medium, it can detect picric acid by turning off fluorescence in the ethanol-water medium. Here actually in ethanol-water medium, the spirolactam ring opening is the main factor to show the fluorescence enhancement in the presence of Hg(II) but this phenomenon is not smooth in less polar DMSO water medium. Here initially the presence of heavy metal forms the complex, reducing the population S1 state. But after a certain period of time, the ring-opening phenomena occur in the DMSO medium which is validated by optical and fluorescence response. After careful handling of the sensing phenomena, the MASS and NMR spectral data analysis are utilized to confirm 1:1 host-guest stoichiometric combination. The DFT study optimizes the structure of the probeanalyte complexes. The biosensing ability of the chemosensor is confirmed by a live cell imaging study. Finally, it is proved that this probe can optically and fluorometrically detect the concentration effect of Hg(II) in real soil samples.

4. Experimental section

4.1. Materials and physical measurements

All the reagents and solvents needed for synthesis are easily accessible on the market. As reagent-grade chemicals were employed throughout the whole experimental section, no additional purification was necessary. Rhodamine B, 1,2-diaminopropane, 5-chlorosalicylaldehyde, and sodium sulfide (Na2S) were purchased from Sigma Aldrich Chemicals. Metals including HgCl2 and Picric acid (PA) were procured from Merck. Perkin-Elmer 240C elemental analyzer was used to conduct elemental analysis. For FTIR data collection ATR mode Bruker Tensor −27 and for electronic absorption study Perkin Elmer UV-Vis Lambda 365 spectrophotometers were used. By using Perkin Elmer Fluorescence spectrometer FL6500 the total fluorescence spectroscopic experiments were performed. The ¹H NMR spectra were recorded in Joel 400 and Bruker Advance 600 operating at 400 MHz and 600 MHz. The particle size of the complexes was measured by Zetasizer Nano ZS90. Scanning Electron Microscopy (SEM) was carried out with a JEOL JSM-6700F field-emission microscope.

4.2. Synthesis of rhodamine-1,2 di amino propene adduct (RBAP)

Rhodamine B (5 \times 10⁻⁴ mol, 0.24 g) and 1,2-diaminopropane (5 \times 10⁻³ mol, 0.45 ml) were dissolved in ethanol. The mixture was refluxed

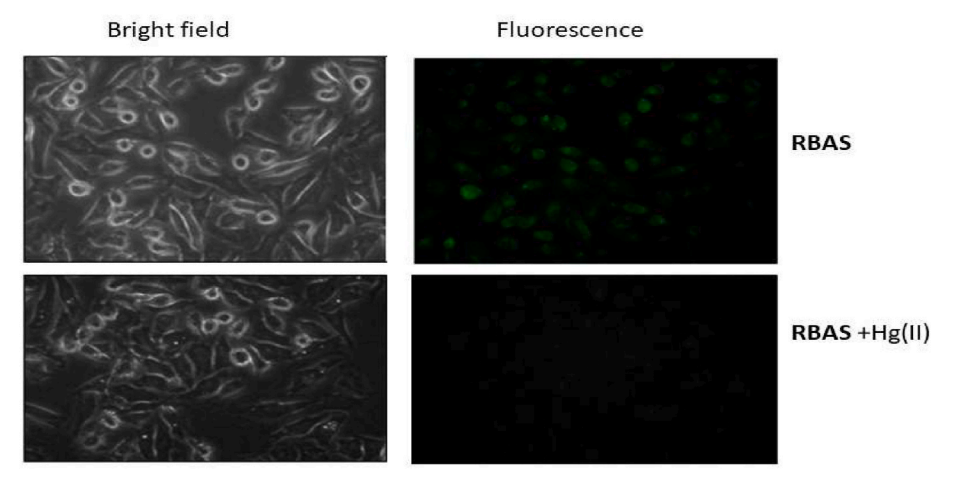


Fig. 11. Fluorescence microscopy images of HeLa cells incubated with RBAS- Hg(II).

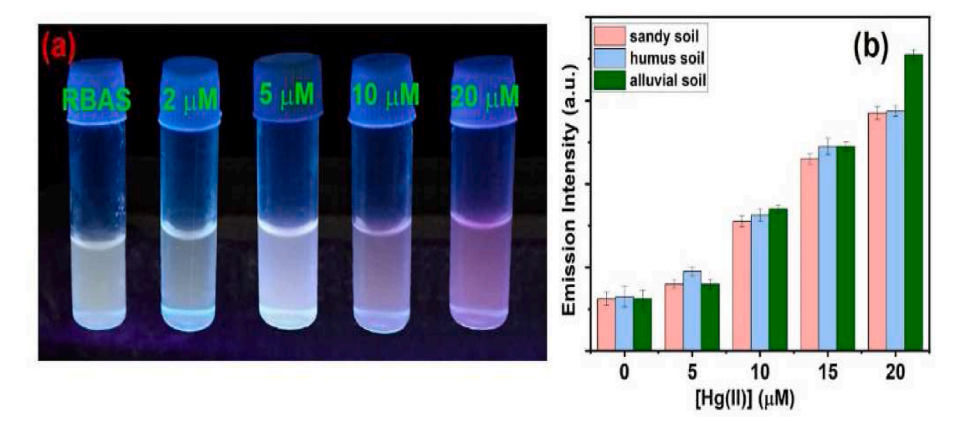


Fig. 12. (a) The pictures of Alluvial soil containing different concentrations Hg(II) after the addition of **RBAS** under the Uv light ($\lambda_{ex} = 365$ nm) (b) change of Emission intensity in the different soil samples after the incorporation of **RBAS** (3×10^{-6} M).

for 16 h. After the solvent was evaporated to dryness under reduced pressure, the crude product was washed with distilled water and collected through filtration followed by centrifugation, then recrystallized from ethanolic solution to remove the impurities, and finally analytical study was performed.

The melting point of RBAS is 97 °C

FT-IR (KBr pellet): ν (C=O) 1686 cm⁻¹, ν (skeletal vibration) 2969 cm⁻¹ ν (C-H stretching)

4.3. UV-vis: 275 nm $(\pi - \pi^*)$, 320 nm $(n - \pi^*)$

 1 H NMR (400 MHz, CDCl₃) δ 7.96–7.90 (m, 1H), 7.51–7.44 (m, 2H), 7.17–7.09 (m, 1H), 6.50–6.40 (m, 1H), 6.39 (s, 3H), 6.30 (t, J=5.6 Hz, 2H), 3.35 (q, J=7.2 Hz, 8H), 3.12 (dd, J=14.2, 8.9 Hz, 1H), 2.94 (dd, J=14.1, 4.8 Hz, 1H), 2.49 (dt, J=12.2, 6.2 Hz, 1H), 1.18 (t, J=7.1 Hz, 12H), 0.88 (d, J=6.4 Hz, 3H).

 ^{13}C NMR (101 MHz, CDCl₃) δ 169.08, 153.61, 153.39, 153.34, 148.98, 148.93, 132.58, 131.44, 128.98, 128.71, 128.21, 124.05, 122.93, 108.35, 108.25, 106.09, 105.78, 97.86, 97.79, 77.48, 77.36, 77.16, 76.84, 65.32, 49.62, 46.18, 44.47, 21.56, 12.73, 12.71.

4.4. Synthesis of RBAS

5-chlorosalicylaldehyde (1 mmol, 0.637 g) was added to the methanolic solution of **RBAP** (1 mmol, 0.499 g) under reflux conditions. Instantaneously, the colorless solution turns yellow. The completion of the reaction was thoroughly monitored by TLC. After the reaction was complete, the solvent was evaporated using a rotary evaporator, and the yellow solid was collected for examination.

4.5. Melting point of RBAS is 195 °C

FT-IR (KBr pellet): ν (C=N) 1616 cm $^{-1}$, ν (skeletal vibration) 1430 cm $^{-1}$ ν (Aromatic C–N stretch) 1374 cm $^{-1}$. UV–vis: 272 nm (π - π *), 318 nm (π - π *).

 1 H NMR (400 MHz, DMSO) δ 12.99 (s, 1H), 7.82 (s, 1H), 7.78–7.75 (m, 1H), 7.54–7.45 (m, 2H), 7.31 (d, J=2.7 Hz, 1H), 7.29 (q, J=2.5 Hz, 2H), 7.03–6.99 (m, 1H), 6.84 (s, 1H), 6.82 (s, 1H), 6.39 (d, J=2.5 Hz, 1H), 6.33 (d, J=2.4 Hz, 1H), 6.28–6.22 (m, 3H), 6.18 (t, J=8.4 Hz, 1H), 3.40 (dd, J=14.1, 8.7 Hz, 2H), 3.26 (q, J=7.4 Hz, 5H), 3.12 (q, J=6.6 Hz, 1H), 2.98 (d, J=4.5 Hz, 1H), 2.95 (d, J=4.5 Hz, 1H), 1.08 (dt, J=9.8, 6.9 Hz, 13H), 0.97 (d, J=6.4 Hz, 3H).

 ^{13}C NMR (101 MHz, DMSO) δ 167.42, 163.21, 159.08, 153.09, 152.83, 152.66, 148.37, 148.32, 132.80, 131.63, 130.38, 130.31, 128.71, 128.38, 128.33, 123.76, 122.36, 121.68, 119.66, 118.33, 108.15, 107.90, 105.45, 104.66, 97.19, 97.13, 64.15, 61.79, 46.45, 43.62, 40.15, 39.94, 39.73, 39.52, 39.31, 39.10, 38.89, 20.65, 12.40.

4.6. X-ray crystallography

Getting the structures of RBAP and RBAS the single crystal X-ray diffraction (SCXRD) analyses study was carried out using Bruker D8 QUEST diffractometer. The crystallographic data and refinement parameters of the RBAP and RBAS were condensed in Table S6 in the supporting information file. Reflection data were measured at 296 K, using graphite monochromatic MoKa radiation with a PHOTON-II detector. The collected data were reduced using the program APEX-III and an empirical absorption correction was carried out using SADABS [47]. The structure was solved using direct methods and refined using the full-matrix least-squares method on F2 using the WINGX software package [48,49]. The molecular graphics were made using SHELXT [50]. All non-hydrogen atoms were refined with anisotropic parameters. CIF file of the complex for the structure reported has been deposited with the Cambridge Crystallographic Data Centre (CCDC). Copies of the data can be obtained, free of charge on application to the CCDC, 12 Union Road, Cambridge, CB2 1EZ UK [Fax: 44 (1233) 336 033 e-mail: deposit@ccdc.cam.ac.uk].

4.7. Raw sample preparation for fluorescence and UV spectral study

The stock solution of chemosensor **RBAS** was made in a methanol medium and the stock solution of competitive metal ions (5 \times 10 $^{-3}$ M) was prepared in triple-distilled water utilizing the chloride salts of the metal ions. During total fluorescence and absorption investigation, the optimal amount of **RBAS** (10 $^{-2}$ M) stock solution was added to 2:8 ethanol-water and 2:8 DMSO–water HEPES buffer medium in the quartz optical cell with a 1 cm optical path length in order to properly assess the experimental concentration. Following the addition of the requisite amount of cationic or anionic stock solutions using a micropipette, spectral data were recorded.

4.8. Fluorescence quantum yield measurements

Fluorescence quantum yield (Φ) was determined using quinine sulphate (Φ_R) reference using the following equation.

4.8.1. Fluorescence quantum yields (φ) sample

 $=\Phi_{\rm R}\times A_{\rm S}/A_{\rm R}\times Abs_{\rm R}/Abs_{\rm S}\times \eta s^2/\eta_{\rm R}^2$

Where A denotes the integrated area under the fluorescence curve, Abs refers to absorbance, η stands for the refractive index of the medium and Φ is the fluorescence quantum yield. S and R in subscript represent the respective parameters for the studied sample and reference, respectively [51].

S. Das et al. Dyes and Pigments 222 (2024) 111884

4.9. Sample preparation for SEM

The probe **RBAS** was dispersed in EtOH/H $_2$ O (2:8 v/v) solution and DMSO/H $_2$ O (2:8 v/v) solution for about 20 min. On different glass discs, the scattered solutions were drop-cast. The discs were submitted to an SEM experiment to record the appropriate pictures after being dried under air for one day at room temperature.

4.10. Sample preparation for DLS

One mg of **RBAS** was dispersed separately in various solutions (4 ml) of EtOH – H_2O mixture and DMSO – H_2O mixture The dispersed solution was then kept in a quartz cuvette to investigate the DLS experiment to obtain the size of the particles.

4.11. Computational details

The ground state geometries of the RBAS is measured in ethanol/ DMSO whereas the RBAS-Hg(II) adducts are fully optimized in both AIE solvent and RBAS - PA adduct is fully optimized in EtOH - H₂O solvent using B3LYP exchange-correlation functional, 6-311+G(d,p) basis set for all non-metallic atoms, and Lanl2dz basis set and respective effective core potential for the metal atoms, as implemented in Gaussian 16 program package have been used. Considering the floppy structure of some of the systems, tight convergence criteria along with ultrafine grid for integral calculations and empirical dispersion (GD3) to account for dispersion interactions are used. The stationary points on respective potential energy hypersurfaces obtained from geometry optimization were confirmed to be minima by the evaluation of respective Hessian. After geometry optimization and vibrational frequency calculations, the one-photon absorption parameters viz. excitation energies, transition moments, oscillator strength, and orbital contributions to each excitation are calculated at the same level of theory in same solvent. The solvent phase environment is mimicked by employing the polarizable continuum model implemented in Gaussian 16 program.

4.12. Sample preparation for the detection of soil samples

Three different types of soil samples were collected from our institute and different areas. At first, the soil samples are dried under sunlight and ground into fine powders. Then 4 ml of Hg(II) solution at different concentrations (0, 5, 10, 20 μM) was mixed with the soil samples and then again dried. After that 0.5 g of each sample was transferred to a 4 ml water solution containing 5.0 μM RBAS separately and stirred for 10 min then allowed to settle. The sediments were moved to the lower part and the clear solution of the upper part was collected very carefully and fluorescence spectroscopic response was monitored.

4.13. Fluorescence imaging study

HeLa cells were seeded in a 24 well cell culture plate at a density of 5 \times 10^4 cells per well using Dulbecco's Modified Eagle's medium (DMEM) supplemented with 10 % Foetal bovine serum (FBS). As a next step, cells were incubated at 37 $^{\circ}\text{C}$ in an atmosphere of air with 5 % CO $_2$ for overnight. The cultured media were separated and then cells were washed with phosphate-buffered saline (PBS, pH 7.4) twice. The cells were then incubated with detector **RBAS** in PBS [25 mM stock solution of **RBAS** was prepared by dissolving it in DMSO; use 1 μL of stock to 500 μL of PBS to obtain 50 μM final concentration of **RBAS**] with PBS (pH 7.4) for 2 h and then added ZnCl $_2$ and washed with PBS. After that under a fluorescence microscope (DeWinter) the cells were observed under 400X magnification and by microscope camera, images were taken. In the next step, ATP was added and microscopic images were collected. Finally, the images were analyzed using Image J 1.49 v software.

4.14. In vitro cytotoxicity assay

The antiproliferative effect of **RBAS** was checked on HeLa cells (human cervical carcinoma cell line) by implementing 3-(4,5-Dimethylthiazol-2-yl)-2,5-Diphenyltetrazolium Bromide (MTT) assay. The 25 mM stock solution of **RBAS** was prepared in DMSO. Initially, the Cells were seeded at a density of 2×10^5 cells/well in a 96-well cell culture plate. After 24 h of cell seeding, cells were exposed to ligand with different concentrations after 4 h of serum starvation. 0.4 % of DMSO in a complete medium was used as a solvent control. After 24 h of incubation, cells were treated with 0.5 mg mL⁻¹ MTT solution (Sigma; prepared in PBS at a concentration of 5 mg mL⁻¹ and diluting in serumfree medium at a final concentration of 0.5 mg mL⁻¹) and then incubated for 3 and a half hrs at 37 °C. The media was removed and the formazan was dissolved in DMSO and OD was measured at 570 nm using a microplate reader (Biorad). The rate of survival was measured by utilizing the following formula [52,53].

Cell viability (%) = $(ODAT / ODAC) \times 100$

Where $OD_{AT} = Absorbency$ of control cells and $OD_{AC} = Absorbency$ of treated cells.

CRediT authorship contribution statement

Susmita Das: Methodology. Manik Das: Methodology. Uttam Kumar Das: Data curation, Software. Bidhan Chandra Samanta: Formal analysis. Arijit Bag: Software. Anutosh Patra: Methodology. Nandan Bhattacharya: Data curation. Tithi Maity: Conceptualization, Supervision, Writing – original draft.

Declaration of competing interest

There are no conflicts of interest to mention.

Data availability

No data was used for the research described in the article.

Acknowledgments

The corresponding author (TM) expresses gratitude to the college authority of Prabhat Kumar College, Contai for their continuous support. TM acknowledges Department of Science and Technology and Biotechnology, Government of West Bengal for the financial support through the Gobeshonay Bangla Scheme. TM is also grateful to DST FIST for the financial support to the Colleg.

Appendix A. Supplementary data

Supplementary data to this article can be found online at https://doi.org/10.1016/j.dyepig.2023.111884.

References

- Jayshankar M, Tseten T, Anbalagan N, Mathew BB, Beeregowda N. Toxicity, mechanism and health effects of some heavy metals. Interdiscipl Toxicol 2014;7: 60–72.
- [2] Zhang D, Wang L, Zeng H, Yan P, Nie J, Sharma VK, Wang C. A three-dimensional macroporous network structured chitosan/cellulose biocomposite sponge for rapid and selective removal of mercury(II) ions from aqueous solution. Chem Eng J 2019; 363:192–202.
- [3] Pacyna EG, Pacyna JM, Sundseth K, Munthe J, Kindbom K, Wilson S, Maxson P. Global emission of mercury to the atmosphere from anthropogenic sources in 2005 and projections to 2020. Atmos Environ 2010;44:2487–99.
- [4] Edwards BA, Kushner DS, Outridge PM, Wang F. Fifty years of volcanic mercury emission research: knowledge gaps and future directions. Sci Total Environ 2021; 757:143800.
- [5] Budnik LT, Casteleyn L. Mercury pollution in modern times and its socio-medical consequences. Sci Total Environ 2019;654:720–34.

- [6] Nath S, Pathak SK, Pradhan B, Gupta RK, Reddy KA, Krishnamoorthy G, Achalkumar AS. A sensitive and selective sensor for picric acid detection with a fluorescence switching response. New J Chem 2018;42:5382–94.
- [7] Zheng W, Zhao Y, Lin X, Zhang Q, Xiao K, Cheng N, Mei X, Lu Y, Yao Z. Rapid and selective detection of picric acid based on supramolecular self-assembly of a cationic perylene diimide in pure aqueous media. Dyes Pigments 2022;207: 110761.
- [8] Gonzales APS, Firmino MA, Nomura CS, Rocha FRP, Oliveira PV, Gaubeur I. Peat as a natural solid-phase for copper precincentration and determination in a multicommuted flow system coupled to flame atomic absorption spectrometry. Anal Chim Acta 2009;636:198–204.
- [9] Farhi A, Firdaus F, Saeed H, Mujeeb A, Shakir M, Owais M. A quinoline-based fluorescent probe for selective detection and real-time monitoring of copper ions—a differential colorimetric approach. Photochem Photobiol Sci 2019;18:3008–15.
- [10] Li CR, Li SL, Wang GG, Yang ZY. Spectroscopic properties of a chromone-fluorescein conjugate as Mg2+ "turn on" fluorescent probe. J Photochem Photobiol Chem 2016;356:700-7.
- [11] Ghosh M, Ghosh A, Ta S, Matalobos JS. ESIPT-Based nanomolar Zn2+ sensor for human breast cancer cell (MCF7) imaging. ChemistrySelect 2017;2:7426–31.
- [12] Udhayakumari D, Velmathi S, Sung Y, Wu S. Highly fluorescent probe for copper (II) ion based on commercially available compounds and live cell imaging. Sensor Actuator B Chem 2014;198:258–93.
- [13] Dodani SC, He Q, Chang CJ. A turn-on fluorescent sensor for detecting nickel in living cells. J Am Chem Soc 2009;131:18020-1.
- [14] Kursunlu AN, Gular E. Novel fluorescent sensor for silver (I) based on the 3,4-bis-triazole Bodipy via dual-click chemistry. J Mol Struct 2017;1134:345–9.
- [15] Oguz M, Kursunlu AN, Yilmaz M. Low-cost and environmentally sensitive fluorescent cellulose paper for naked-eye detection of Fe (III) in aqueous media. Dyes Pigments 2020;173:107974.
- [16] Alizada M, Gul A, Oguz M, Kursunlu AN, Yilmaz M. Ion sensing of sister sensors based-on calix [4] arene in aqueous medium and their bioimaging applications. Dyes Pigments 2021;184:108741.
- [17] Diana R, Caruso U, Costanzo LD, Gentile FS, Panunji B. Colorimetric recognition of multiple first-row transition metals: a single water-soluble chemosensor in acidic and basic conditions. Dyes Pigments 2021;184:108832.
- [18] Zhang L, Hu W, Yu L, Wang Y. Click synthesis of a novel triazole bridged AIE active cyclodextrin probe for specific detection of Cd²⁺. Chem Commun 2015;51: 4208–201
- [19] Samanta S, Goswami S, Hoque MN, Ramesh A, Das G. An aggregation-induced emission (AIE) active probe renders Al(iii) sensing and tracking of subsequent interaction with DNA. Chem Commun 2014;50:11833–6.
- [20] Diana R, Panunji B. Zinc (II) and AIEgens: the "clip approach" for a novel fluorophore family. A Review. Molecules 2021;26:4176.
- [21] Wu J, Liu W, Ge J, Zhang H, Wang P. New sensing mechanisms for design of fluorescent chemosensors emerging in recent years. Chem Soc Rev 2011;40: 2422-05.
- [22] Wang Z, Zhou F, Gui C, Wang J, Zhao Z, Qin A, Tang BZ. Selective and sensitive fluorescent probes for metal ions based on AIE dots in aqueous media. J Mater Chem C 2018;6:11261–5.
- [23] Luo J, Xie Z, Lam JW, Cheng L, Chen H, Qiu C, Kwok HS, Zhan X, Liu Y, Zhu D. Aggregation-induced emission of 1-methyl-1,2,3,4,5-pentaphenylsilole. Chem Commun 2001:1740–1.
- [24] Jiang R, Liu N, Li F, Fu W, Zhou Y, Zhang Y. Novel PSMA-coated On-Off-On fluorescent chemosensor based on organic dots with AIEgens for detection of copper (II), iron (III) and cysteine. Polymers 2018;10:786–94.
- [25] Tharmalingam B, Mathivanan M, Dhamodiran G, Mani KS, Paranjothy M, Murugesapandian B. Star-shaped ESIPT-active mechanoresponsive luminescent AIEgen and its on-off-on emissive response to Cu2+/S2. ACS Omega 2019;4: 12459-69.
- [26] Yuan Y, Chen X, Chen Q, Jiang G, Wang H, Wang J. New switch on fluorescent probe with AIE characteristics for selective and reversible detection of mercury ion in aqueous solution. Anal Biochem 2019;585:113403.
- [27] Balamurugan G, Velmathi S, Thirumalaivasan N, Wu SP. New phenazine based AIE probes for selective detection of aluminium(iii) ions in presence of other trivalent metal ions in living cells. Analyst 2017;142:4721–6.
- [28] Fang W, Zhang G, Chen J, Kong L, Yang L, Bi H, Yang J. An AIE active probe for specific sensing of Hg2+ based on linear conjugated bis-Schiff base. Sens Actuators, B 2016;229:338–46.
- [29] Kan C, Shao X, Song F, Xu J, Zhu J, Du L. environment. Bioimaging of a fluorescence rhodamine-based probe for reversible detection of Hg (II) and its application in real water environment. Microchem J 2019;150:104142.
- [30] Wang Y, Wang Y, Guo F, Wang Y, Xie P. A new naked-eye fluorescent chemosensor for Cu (II) and its practical applications. Res Chem Intermed 2021;47:3515–28.

- [31] Kursunlu AN, Oguz M, Yilmaz M. On/off rhodamine-BODIPY-based fluorimetric/ colorimetric sensor for detection of mercury (II) in half-aqueous medium. IEEE Sensor J 2018:19:2009–15.
- [32] Paul S, Bhuyan S, Mukhopadhyay SK, Murmu NC, Banerjee P. Aggregation-induced modulation of the optoelectronic properties of carbon dots and removal of Cd2+ ions with sustainable use in photocurrent generation. ACS Sustainable Chem Eng 2019;7:13687–97.
- [33] Karaku S. A rhodamine based fluorescent chemodosimeter for the selective and sensitive detection of copper (II) ions in aqueous media and living cells. J Mol Struct 2021;1224:129037.
- [34] Cicekbilek F, Yilmaz B, Bayrakci M, Gezici O. An application of a schiff-base type reaction in the synthesis of a new rhodamine-based Hg (II)-sensing agent. J Fluoresc 2019;29:1349–58.
- [35] Patil SK, Das D. A nanomolar detection of mercury(II) ion by a chemodosimetric rhodamine-based sensor in an aqueous medium: potential applications in real water samples and as paper strips. Spectrochim Acta Part A Mol Biomol Spectrosc 2019;210:44–51.
- [36] Doumani N, Bou-Maroun E, Maalouly J, Tueni M, Dubois A, Bernhard C, Denat FP, Sok N, Cayot. A new pH-dependent macrocyclic rhodamine B-based fluorescent probe for copper detection in white wine. Sensors 2019;19:4514.
- [37] Ghosh P, Kumar N, Mukhopadhyay SK, Banerjee P. Sensitive and fluorescent Schiff base chemo sensor for pico molar level fluoride detection: in vitro study and mimic of logic gate function. Sensor Actuator B Chem 2016;224:899–906.
- [38] Das P, Rajput SS, Das M, Laha S, Choudhuri I, Bhattachatyya N, Das A, Samanta BC, Alam MM, Maity T. Easy, selective and colorimetric detection of Zn(II), Cu(II), F– ions by a new piperazine based Schiff base chemosensor along with molecular logic gate formation and live cell images study. Photochem. Photobiol A Chem 2022; 427:113817.
- [39] Dey S, Sarkar S, Maity D, Roy P. Rhodamine based chemosensor for trivalent cations: synthesis, spectral properties, secondary complex as sensor for arsenate and molecular logic gates. Sensor Actuator B Chem 2017;246:518–34.
- [40] Yang QZ, Wu LZ, Zhang H, Chen B, Wu ZX, Zhang LP, Tung CHA. Luminescent chemosensor with specific response for Mg2+. Inorg Chem 2004;43:5195-7.
- [41] Nijegorodov NI, Downey WS. The influence of planarity and rigidity on the absorption and fluorescence parameters and intersystem crossing rate constant in aromatic molecules. J Phys Chem 1994;98:5639–43.
- [42] Shyamal M, Mazumdar P, Maity S, Samanta S, Sahoo Gp, Mishra A. Highly selective turn-on fluorogenic chemosensor for robust quantification of Zn(II) based on aggregation induced emission enhancement feature. ACS Sens 2016;1:739–47.
- [43] Kim HN, Lee MH, Kim HJ, Kim JS, Yoon J. A new trend in rhodamine-based chemosensors: application of spirolactam ring-opening to sensing ions. Chem Soc Rev 2008;37:1465–72.
- [44] Mandal J, Ghorai P, Pal K, Bhaumik T, Karmakar P, Saha A. Development of rhodamine 6G-based fluorescent chemosensors for Al3+-ion detection: effect of ring strain and substituent in enhancing its sensing performance. ACS Omega 2020; 5:145-57.
- [45] Leite A, Silva AMG, Silva LC, de Castro B, Gameiro P, Rangel M. Discrimination of fluorescence light-up effects induced by pH and metal ion chelation on a spirocyclic derivative of rhodamine B. Dalton Trans 2013;42:6110–8.
- [46] Wang E, Zhou Y, Huang Q, Pang L, Qiao H, Yu F, Gao B, Zhang J, Min Y, Ma T. 5-Hydroxymethylfurfural modified rhodamine B dual-function derivative: highly sensitive and selective optical detection of pH and Cu2+. Spectrochim Acta Mol Biomol Spectrosc 2016:152:327–35.
- [47] Sheldrick GM. SADABS, program for empirical absorption correction of area detector data. Germany: University of Gottingen; 1996.
- [48] Farrugia LJ. WINGX—a windows program for crystal structure analysis. Glasgow: University of Glasgow; 1998.
- [49] Farrugia LJ. WinGX suite for small-molecule single-crystal crystallography. J Appl Cryst 1999;32:837–8.
- [50] Sheldrick GM. SHELX—a program for automatic solution of crystal structures. Germany: University of Gottingen; 1997.
- [51] Jana A, Sukul PK, Mandal SK, Konar S, Ray S, Das K, Golen JA, Rheingold AL, Mondal S, Mondal TK, Khuda-Bukhsh AR, Kar SK. A novel 2,6-diformyl-4-methylphenol based chemosensor for Zn(ii) ions by ratiometric displacement of Cd(ii) ions and its application for cell imaging on human melanoma cancer cells. Analyst 2014;139:495–504.
- [52] Goswami S, Maity S, Maity AC, Das AK, Khanra K, Mandal TK, Bhattacharyya N. A macrocyclic piperazine linked extremely Zn2+ selective fluorescent chemosensor with bio-imaging and for H2PO4- sensing. Tetrahedron Lett 2014; 55:5993-7.
- [53] Scherer WF, Syverton JT, Gey GO. Studies on the propagation in vitro of poliomyelitis viruses. J Exp Med 1953;97:695–710.